Biogeotechnics 4 (2026) 100145

Contents lists available at ScienceDirect

Biogeotechnics

journal homepage: www.keaipublishing.com/en/journals/biogeotechnics/

Research Article

Study on the pullout bearing characteristics of bio-inspired root piles in coral sand foundation under different root buried depths

Xiangwei Fang[a,b,c], Yaoyi Zhang[a,d], Zhiqiang Wang[a,e,*], Peixi Xiong[f], Fenghui Hu[a], Ganggang Zhou[a], Chunyan Wang[a,b,c]

[a] School of Civil Engineering, Chongqing University, Chongqing 400045, China
[b] State Key Laboratory of Safety and Resilience of Civil Engineering in Mountain Area, Chongqing 400045, China
[c] Innovation Center for Biogenic Construction Technology, Chongqing University, Chongqing 400045, China
[d] CCCC Yangtze River Construction Development Group Co., Ltd., Chongqing 400021, China
[e] School of Civil Engineering, Tianjin University, Tianjin 300354, China
[f] Undergraduate School, Chongqing University, Chongqing 400044, China

ARTICLE INFO

Keywords:
Bio-inspired root piles (Root pile)
Coral sand
Pullout resistance
Root buried depth
Bearing characteristic

ABSTRACT

Bio-inspired root pile (abbreviated as root pile) is a new type of bio-inspired foundation, which has a broad application prospect in the development and construction of China's South China Sea area due to its good bearing characteristics such as pullout bearing capacity. The effect of root buried depth on the uplift bearing characteristics of root piles is analyzed through the model test of uplift bearing of root piles with different root buried depths in coral sand foundation. The results show that increasing the root buried depth can improve the ability of the root pile to control the uplift displacement, and there exists an optimal buried depth or range of buried depths that can effectively improve the pile foundation's uplift bearing capacity and control the ultimate displacement. The attenuation of axial force at the root is in the form of a step; with the increase of root buried depth, the maximum value of lateral friction resistance develops from the lower part of the pile body without root to the upper part of the pile body without root. The range of the bearing ratio of the root section of the pile with root buried depth of 260 mm, 340 mm and 420 mm is 12.33%–15.68%, 9.98%–17.82% and 7.61%–21.65%, respectively; the smaller the root buried depth is, the higher is the ratio of the bearing ratio of the root section at the beginning of loading, and the bigger the root buried depth is, the bigger is the ratio of the root's final bearing ratio. The change of soil pressure around the pile increases and then decreases, and the densest point of soil compacting moves upward with the increase of root buried depth. The research results provide scientific basis for the design of root pile buried depth and root arrangement in actual projects.

1. Introduction

Offshore wind is an important renewable energy source (Li et al., 2022). One area that scholars have explored in this regard is the design of offshore wind power facility foundations. Additionally, these foundations may encounter diverse environmental conditions such as coral sand or weak ground foundations. The distinctive engineering properties of coral sand bear significant implications for the safety of offshore structures (Fang et al., 2015, 2023, Hu et al., 2023a, 2023b; Peng et al., 2021; Wang et al., 1997). Optimizing the foundation design for offshore wind power generation facilities in coral sand settings has become a significant research focus. This optimization aims to fulfill requirements pertaining to load-bearing capacity and cost-effectiveness.

Bio-inspired root pile (abbreviated as root pile) is a new type of bio-inspired foundation, which is formed by mimicking the roots of a tree by pushing a root into the sidewall of the pile (Yin, 2007). The design calculation of root piles in actual projects mainly involves bearing capacity, displacement and root arrangement. The root arrangement includes the number of layers of root, the spacing between layers of root, the number of roots in each layer and the buried depth of root. Therefore, scholars have carried out a large number of field tests, numerical simulations and theoretical researches around the actual project, and investigated the characteristics of root piles under different

* Corresponding author.
E-mail address: nchucquwzq@163.com (Z. Wang).

https://doi.org/10.1016/j.bgtech.2024.100145
Received 17 June 2024; Received in revised form 22 September 2024; Accepted 16 October 2024
Available online 22 October 2024
2949-9291/© 2026 The Authors. Publishing services by Elsevier B.V. on behalf of KeAi Communications Co. Ltd. This is an open access article under the CC BY-NC-ND license (http://creativecommons.org/licenses/by-nc-nd/4.0/).

loads, different foundation properties and different root arrangements. (Gong et al., 2015; Luo et al., 2022a, 2022b; Mu et al., 2010; Wang et al., 2024; Zhou et al., 2021). Regarding the root pile bearing mechanism, Zhang et al. (2020) presented the distribution of root pile resistance to pullout displacement field through transparent soil model tests, which elucidated the root pile bearing mechanism. In the theoretical study of root foundation design calculation, Luo et al. (2022a, 2022b) developed a modified hyperbolic load transfer model for nonlinear settlement analysis of root piles in multilayer soil. This was followed by the introduction of an extended beam model of nonlinear Winkler foundation (BNWF) that considers soil-root interactions for analyzing the nonlinear behavior of root foundations under transverse loads in 2022. Yu et al. (2023) proposed a root foundation compressive damage mode, which served as the basis for deriving the formula to calculate the compressive ultimate bearing capacity of root foundations. Hu et al. (2010) derived an elastic solution for the bearing performance of root sinkholes containing bent roots by incorporating root bending and overlap folding effects into the load transfer method and the Winkler foundation beam theory (Hu et al., 2010; Luo et al., 2022a, 2022b; Yancheng et al., 2023). Building on experimental results, Wang et al. (2024) put forward three types of root foundation pullout damage modes. Subsequently, they developed the formula for calculating the root foundation pullout bearing capacity. With respect to the root foundation pullout bearing characteristics, Wang et al. (2023) and Fang et al. (2024) investigated the impact of relative foundation compaction, foundation water content state, and the number of root layers on the root pile pullout bearing characteristics in coral sand foundations. The current research on root foundations mainly focuses on the vertical, horizontal and joint bearing characteristics of root foundations in loess, clay, silty sand and coral sand foundations. The depth of root is an important design parameter for the design calculation of root piles. If the depth of root is too shallow, the bearing capacity of root piles will be low, and if it is too deep, it will affect the number of layers of root and thus reduce the bearing capacity of root piles. The existing studies have not considered the effect of root depth on the bearing characteristics of root foundation, and the reasonable range of root depth is an important issue to be solved in the design calculation of root pile. In addition, coral sand foundations have special engineering mechanical properties, and no research has been reported on the bearing characteristics of root piles in coral sand foundations with different root buried depths.

The primary loads acting on the foundations of offshore structures, such as offshore wind turbine power generation, are scouring and uplift forces induced by wind and seawater. Piles, serving as typical uplift-resistant foundations, have been extensively utilized in marine engineering. Predicting the uplift capacity and displacement of uplift-resistant piles is a crucial aspect of engineering design, and researchers have undertaken numerous investigations on various types of piles (Aamer et al., 2023; Lei et al., 2022; Liu et al., 2011; Malik et al., 2019; Moayedi & Mosallanezhad, 2017; Moayedi & Rezaei, 2019; Qi et al., 2015; Vignesh & Muthukumar, 2023; Zhang et al., 2018). Liu et al. (2023) formulated a theoretical prediction equation for the ultimate uplift capacity of a single pile based on the Hoek-Brown criterion. Apart from equal-diameter piles, anchor piles, helical piles, flared-bottom piles, and extruded flared support disk piles are commonly employed as pullout-resistant piles. Anchor piles find wide application in mariculture. Gui et al. (2021) analyzed the impact of initial tension angle, pile diameter, buried depth, and pile type on the pullout resistance of anchor piles under inclined loads. Vignesh and Muthukumar (2023) examined the pullout resistance and horizontal properties of helical pile groups in soft soils using finite element modeling, proposing an optimal spacing ratio between pullout-resistant grouped piles and horizontal grouped piles. Moayedi and Rezaei (2019) devised a formula for calculating the ultimate pullout capacity of spread base piles in cohesionless soils based on an artificial neural network model. The fundamental concept behind research on resistant piles mirrors that of compressive piles, focusing on observing the bearing deformation characteristics of the pile foundation, exploring its bearing mechanism, and ultimately establishing a design calculation approach to predict its bearing deformation (Moayedi & Rezaei, 2019; Qi et al., 2015; Ma et al., 2020, 2023; Polishchuk and Maksimov, 2018; Yao and Chen, 2014; Yao and Xiao, 2019). The buried depth of roots is a pivotal parameter for designing and calculating root piles, significantly influencing their pullout bearing properties. Notably, investigations on the buried depth of roots in coral sand foundations are scarce.

To summarize, the current research on pullout piles mainly focuses on the pullout bearing capacity and deformation law of various types of profiled piles, but the pullout bearing characteristics of root piles in coral sand foundation with different root buried depths have not yet been reported in the research. In this paper, we analyze the pullout bearing characteristics of root piles in coral sand foundation through model test to reveal the bearing mechanism of root piles, which can provide scientific basis for the design of root piles' buried depth and the arrangement of root piles in actual projects, and it is of great significance to promote the development and application of root foundation.

2. Material and methods

2.1. Coral sand

The coral sand used in the experiment was consistent with the previous study (Wang et al., 2023, 2024; Fang et al., 2024), which was taken from an island reef in the Chinese waters, and the grain size composition is shown in Fig. 1A, and the physical parameters are shown in Table 1.

2.2. Test model device

The test setup comprises five components: a stand, model box, loading device, load transfer apparatus, and stabilizing mechanism, as illustrated in Fig. 1B and G. The stand functions as a crane, while the model box is a rectangular structure with internal dimensions of 1 m × 0.8 m × 0.8 m (length × width × height). The loading device consists of a weight, and the load transfer apparatus involves a 3 mm steel wire and a fixed pulley. Additionally, a counterweight attached to the crane serves as the stabilizing mechanism to prevent tipping over.

The similar material of the model pile adopts plexiglass, the density and other parameters of this kind of material can better meet the requirements of the model test, and the deformation is easy to measure, the density of plexiglass is 1180 kg/m^3, the modulus of elasticity E is 2.5 GPa, Poisson's ratio ν is 0.367. This test adopts three root piles with 1-layer root, shown in Fig. 1D–F, and the buried depth of the root is 260 mm, 340 mm and 420 mm, and the diameter is 40 mm. The length of the root pile is 550 mm, and the diameter is 40 mm, the model box size and pile size meet the requirements of boundary effect (Wang et al., 2024). The dimensions of the model box and the pile dimensions satisfy the requirements of the boundary effect (Wang et al., 2024). The detailed dimensions of the root are shown in Fig. 1I, and the root exposed outside the pile body is a rectangular body with length × width × height of 15 mm × 6 mm × 6 mm (Wang et al., 2024). The construction process of the root pile can be mainly divided into four steps: digging the hole, lowering the steel0bar cage, jacking the root, and pouring the concrete. Among them, the root jacking can be done by mechanical jacking and manual jacking, and the mechanical jacking can be divided into two ways based on the construction platform jacking and fully mechanized single-arm device jacking (Yin, 2015). From the aforementioned construction steps, it can be seen that the root is bonded to the pile body by concrete, which can be simplified to a fixed end.

The model test data acquisition system includes a data acquisition box, an earth pressure box, a strain gauge and a displacement

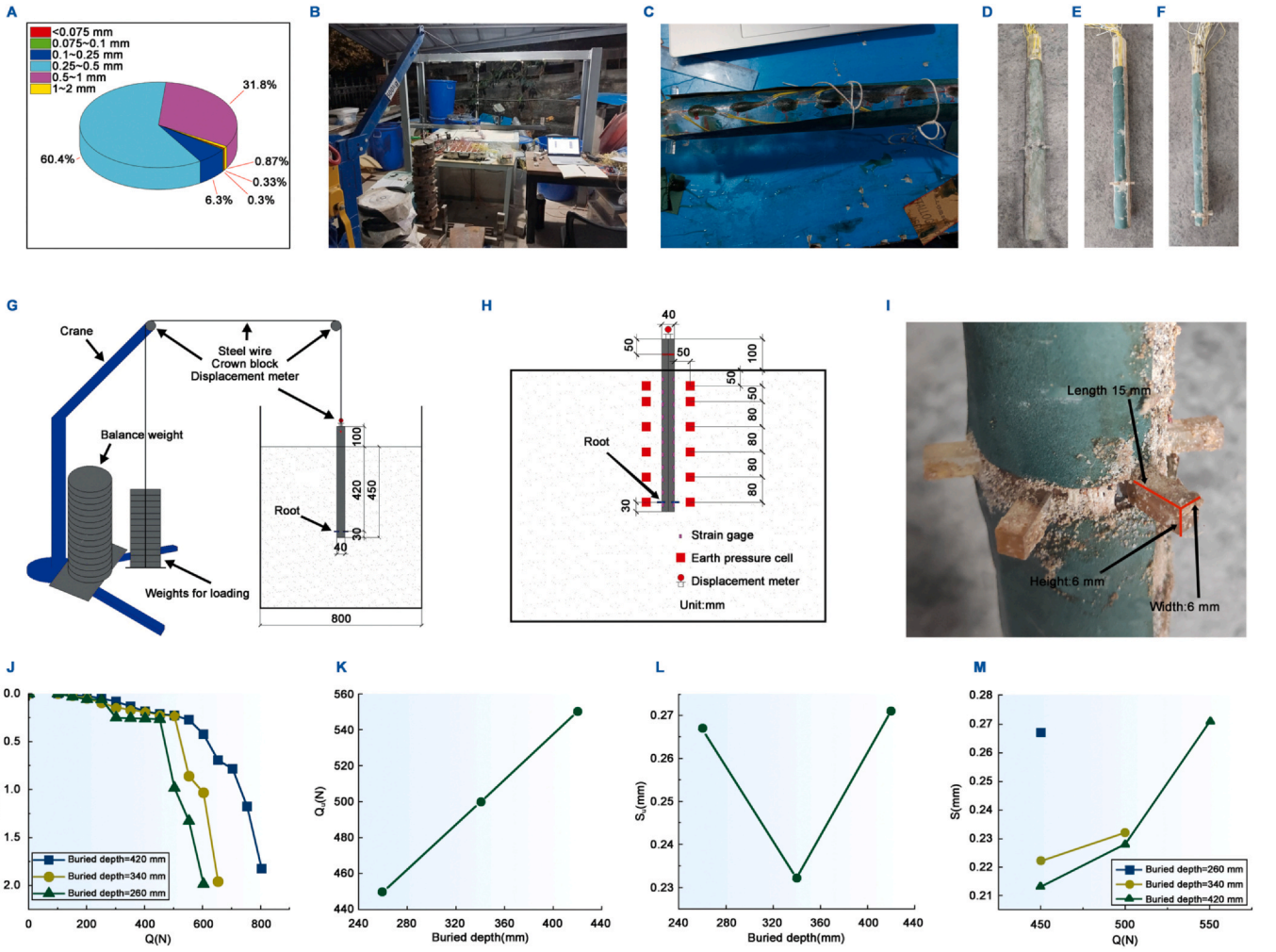

Fig. 1. (**A**) Proportion of soil grains in each grain group; Test model device diagram (Wang et al., 2024): (**B**) Physical diagram of the test setup, (**G**) Schematic diagram of the uplift device; (**C**) 1 layer of AB adhesive on the surface of the strain gage and the interface treatment with the pile body; Test piles for the study of the effect of root buried depth on the pullout bearing characteristics of root piles: (**D**) The root buried depth is 260 mm, (**E**) The root buried depth is 340 mm, (**F**) The root buried depth is 420 m (Wang et al., 2024); (**H**) Sensor layout of root piles; (**I**) Detailed dimensional drawing of root (Wang et al., 2024); (**J**) Q-S curves of root piles with different root buried depths; (**K**) Relation curve between ultimate pulling capacity Q_u and buried depth of root; (**L**) Relation curve between ultimate displacement S_u and root buried depth; (**M**) Displacement curves of pile tops for each pile subjected to ultimate uplift loads for other working conditions.

Table 1
Physical parameters of coral sand (Wang et al., 2023).

G_s	C_u	C_c	d_{10}	d_{30}	d_{60}	e_{max}	e_{min}
2.78	1.77	0.91	0.26	0.33	0.46	1.14	0.68

gauge. The earth pressure box used in this paper is the BWM type (miniature) earth pressure sensor produced by Chaoyuan Instrument Factory in Liyang City, with a diameter of 16 mm and a measuring range of 1 MPa, which can work in saturated water environment. The bottom end of the buried earth pressure box is rammed with soil, and the upper part is covered with a layer of fine sand, which is used to measure the earth pressure of the foundation soil layer. The strain gauge is BE120–3AA-P3k resistance strain gauge manufactured by AVIC Electrical Measuring Instruments Co., LTD. The resistance value is 119.9 ± 0.1 Ω and the sensitivity coefficient is 2.17 ± 1%. Displacement meter is used to measure pile top displacement. The displacement meter used in this model test is the TST-50 strain gauge displacement meter produced by Jiangsu Teste Electronic Equipment Manufacturing Co., LTD., with a measuring range of ± 25 mm and a sensitivity of 0.12733 mV/mm. It is characterized by high sensitivity and good stability.

2.3. Similarity ratio of the model

The model test is designed according to the second theorem of similarity, and the similar parameters are taken as geometry, pile density, acceleration, force, stress and pile elastic modulus. Since it is a static test, it is not possible to completely satisfy the similar indicators, this study focuses on the root pile pullout bearing characteristic law, and the approximate satisfaction of the similar indicators can achieve the purpose of the study. The prototype pile simulated in this model test is made of C40 concrete with density taken as 2430 kg/m^3 and modulus of elasticity taken as 32.5 GPa (Wang et al., 2024). The geometric similarity ratio is taken as 1:40, and the other similarity ratios are calculated through the similarity indexes to obtain the pile density similarity ratio of 2.06, acceleration similarity ratio of 1, force similarity ratio of 18768, stress similarity ratio of 11.73, and elastic modulus similarity ratio of 11.73.

2.4. Testing program

Root piles with 1-layer root with root buried depths of 260 mm, 340 mm and 420 mm were set up for comparative tests with three working conditions. All the piles with 1 layer root are used, and the number of roots in each layer is 6, and the relative compaction of the foundation is 0.65. The test program is shown in Table 2.

Table 2
The effect of different root buried depth on the pullout capacity of root piles test group.

Case	Pile type	Buried depth(mm)
1	Root pile	420
2	Root pile	340
3	Root pile	260

Note: The buried depth of a root is the distance of the midpoint of the root in the height direction from the surface of the foundation.

The data acquisition system consists of a data acquisition box, a computer, sensors, and wires. The data acquisition box visualizes the signals from the sensors as various data plots on the computer through the wires. The arrangement of earth pressure box, strain gauges and displacement gauges are shown in Fig. 1H.

2.5. Testing procedure

The test process mainly includes: ① Strain Gauge Adhesion: Adhesive 1 layer of AB adhesive on the outer surface of strain gauges to ensure that the strain gauges are not damaged during the test, as shown in Fig. 1C (Wang et al., 2024); ② Pile Interface Processing: Adhesive 1 layer of W50 sandpaper on the pile body, and coral sand at the root to simulate the contact between the pile-soil interface, as shown in Fig. 1C (Wang et al., 2024); ③ Checking whether the sensors are working properly; ④ Foundation preparation and sensor placement: The mass of coral sand was calculated according to the measured maximum and minimum dry density of the coral sand and the relative compaction of 0.65 for each layer of coral sand. It was then compacted to the appropriate height. The earth pressure box is buried at the same time as the foundation preparation, and the displacement meter is set at the top of the pile after the foundation preparation is completed; ⑤ Loading, the slow and continuous loading method was adopted, and data collection was started at the same time (Wang et al., 2024).

The loading procedure is shown below (Ministry of Housing and Urban-Rural Development of the People's Republic of China, 2014):

① Graded loading: load according to 50 N for each grade, the first graded load is taken as 2 times of graded load, i.e. 100 N, and each subsequent grade load is 50 N;

② Deformation observation: after each level of loading is applied, record the displacement of pile top at 5 min, 10 min, 15 min, 30 min, 60 min, 90 min and 120 min after loading;

③ When the settlement rate of pile top reaches the relative stability standard, the next level of loading can be applied. Relative stability criterion of test pile: the settlement of pile top shall not exceed 0.1 mm in each hour and occur twice consecutively (starting from the 30th min after the application of graded load, calculated according to the settlement observation value of every 30 min for three consecutive 1.5 h);

④ After the pile is pulled out from the soil, then the loading is stopped.

3. Results

3.1. Q-S curve

The Q-S curves of root piles under different root buried depths are shown in Fig. 1J. The Q-S curves of all pull-out piles are of steep drop type, and the ultimate pull-out bearing capacity is the load at the starting point of steep drop (Gong, 2015). The ultimate pull-out bearing capacity Q_u and the corresponding displacement S_u of 1-layer root piles with buried depths of 260 mm, 340 mm and 420 mm are 450 N, 0.267 mm; 500 N, 0.232 mm; and 550 N, 0.271 mm, respectively. The relationship curves of ultimate pullout bearing capacity Q_u, pile top displacement S_u and root buried depth are shown in Fig. 1K and L.

The ultimate pullout capacity Q_u of root piles with root buried depths of 340 mm and 420 mm increases by 11.11% and 22.22%, respectively, compared with that of root piles with a root buried depth of 260 mm, as can be seen in Fig. 1K. Q_u also increases significantly with an increase in root buried depth. Fig. 1L shows that as the buried depth grows, the root pile's S_u first falls and subsequently increases. The root pile with the lowest ultimate pullout displacement, measuring 0.232 mm, is the one with a buried depth of 340 mm. It can be seen that there exists the optimum buried depth or range of buried depth that can greatly enhance the pile foundation pullout load capacity and at the same time the ultimate displacement is relatively small. The ultimate displacement corresponding to the ultimate bearing capacity of the pile foundation reflects the displacement control ability of the pile foundation. The smaller the ultimate displacement, the stronger the displacement control ability of the pile foundation. Using the ultimate pulling load Q_u of each pile as the horizontal coordinate and the displacement of the top of each pile under the ultimate pulling load Q_u as the vertical coordinate, a curve is drawn, as shown in Fig. 1M. The picture shows that when the load is 450 N and the buried depth of the root increases, the top displacement of the three model piles reduces first quickly and then somewhat. The uplift displacement increments of the root piles with buried depths of 340 mm and 420 mm are close to one another when the load is 500 N. This indicates that while elevating the root buried depth can help the root piles better control the uplift displacement, elevating the root buried depth beyond a certain point has little effect on that ability. The reason for the above phenomenon is that, with the increase of root buried depth, the force of soil acting on the root is larger, and the equivalent lateral friction resistance at the root pile section is higher, on the other hand, the crowding effect of the root on the soil above can also increase the lateral friction resistance of the soil above to the pile body, so increasing the root buried depth can greatly improve the ultimate uplift bearing capacity of the root pile to resist the uprooting. For the uplift displacement and ultimate displacement S_u, the soil resistance and strength at the root will increase when the root buried depth increases, so under the same level of load, the larger the buried depth, the smaller the uplift displacement is, and the ultimate displacement S_u decreases at the beginning of the uplift resistance; When the root pile bears a large ultimate uplift load, the soil under the pile body is fully developed, and the ultimate uplift bearing capacity may be reached during the process of penetrating the plastic zone around the pile. The greater the buried depth of the root, the greater the range of the plastic zone around the pile, and the greater the ultimate uplift displacement S_u. In the actual project, the two factors of uplift bearing capacity and uplift displacement should be comprehensively considered. The buried depth of the root should not be too small. A shallow depth will result in a low uplift bearing capacity of the root pile. However, the buried depth of the root cannot be increased indefinitely. Beyond a certain depth, the improvement in displacement control ability becomes minimal. Moreover, increasing the depth too much may lead to an overstandard uplift displacement. When the root is multi-layered, the spacing between layers and the number of layers will also limit how deep the root can be buried.

3.2. Axial force of pile body

The axial force of the pile body F_N is calculated by first measuring the strain with strain gauges and then calculating according to Formula (1).

$$F_N = EA\varepsilon \tag{1}$$

In the formula, F_N is the axial force of the pile; E is the modulus of elasticity of the pile; A is the cross-sectional area of the equal diameter section of the pile; and ε is the axial strain of the pile.

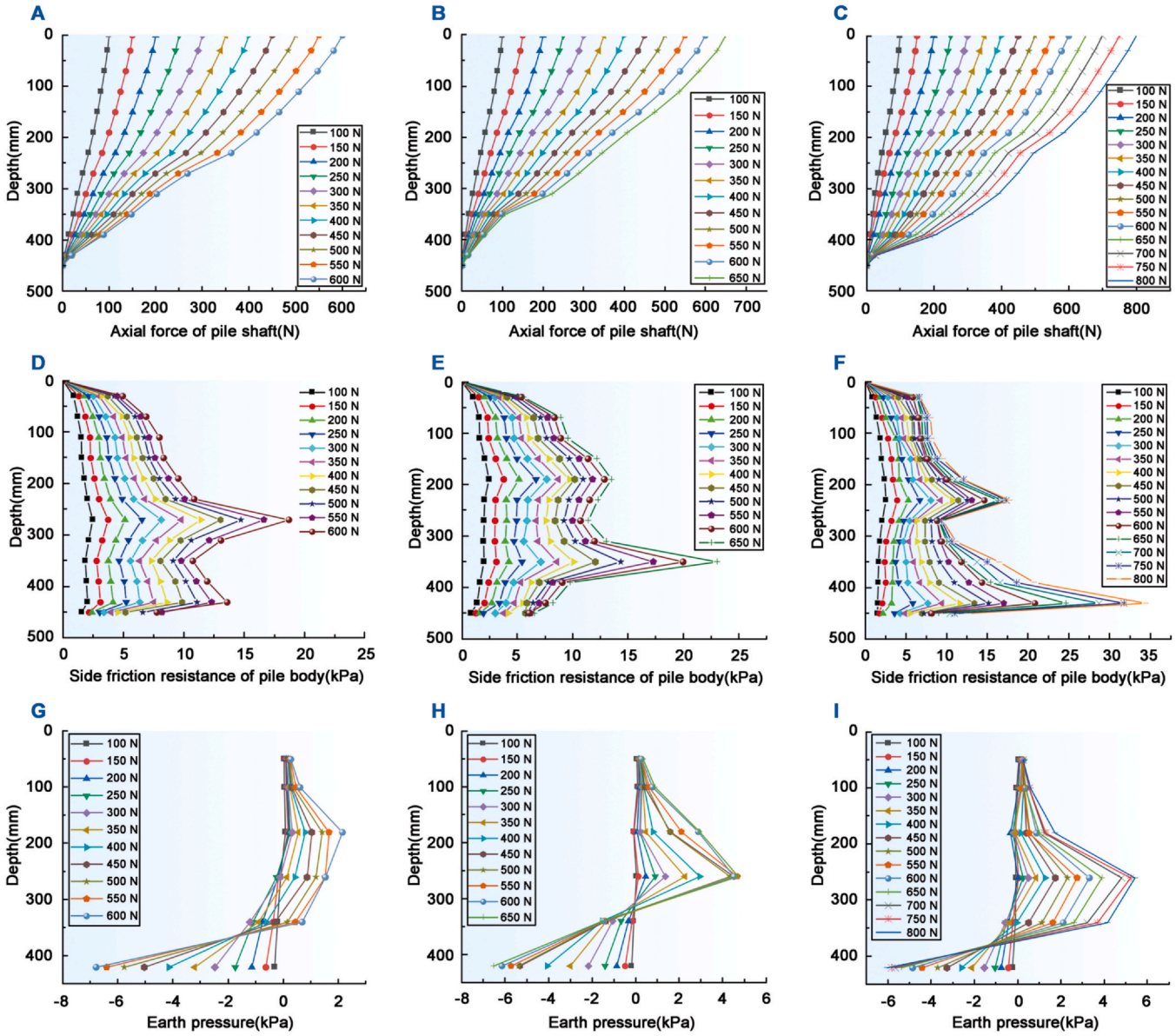

Fig. 2. Axial force diagram of root pile body with different root buried depths: (**A**) Buried depth 260 mm, (**B**) Buied depth 340 mm, (**C**) Buried depth 420 mm; Lateral friction resistance diagram of root pile under different root buried depths: (**D**) Buried depth 260 mm, (**E**) Buried depth 340 mm, (**F**) Buried depth 420 mm; Soil pressure diagram of root pile around the pile for different root buried depths: (**G**) Buried depth 260 mm, (**H**) Buried depth 340 mm, (**I**) Buried depth 420 mm.

The axial force diagrams of piles at different root buried depths are shown in Fig. 2A–C. The axial force of each pile body decays gradually with the increase of depth, and finally decays to 0, and the axial force decays at the root show a step-like shape. The root piles with root buried depths of 260 mm and 340 mm have obvious sharp decay at the root, while the root pile with root buried depth of 420 mm has the largest rate of axial force decay at the root and the middle of the pile body. The reason may be that the lateral friction resistance of the pile body is exerted from the top to the bottom, and the equivalent average lateral friction resistance at the root pile section is larger compared with that at the non-root section, so that the axial force decay at the root section shows a stepped shape. Due to the crowding effect of the root on the soil above, the upper part of the root pile without root at a buried depth of 420 mm formed a great value of lateral friction resistance, i.e., the value of lateral friction resistance at the densest point of the soil around the pile, so the root pile with a buried depth of 420 mm had the greatest rate of axial force attenuation at the root and at the middle of the pile body.

3.3. Frictional resistance along the pile body

The pile body is divided into 12 segments, and the pile lateral friction resistance is the equivalent average lateral friction resistance of each pile segment, which consists of the lateral friction resistance of the equal diameter segments of the pile body and the resistance due to the root, and is calculated as shown in Formula (2).

$$q_{sij} = \frac{F_{ij}}{A_j} \tag{2}$$

In the formula, q_{sij} denotes the equivalent average lateral friction resistance of pile section j for load level i; F_{ij} denotes the axial force attenuation of pile section j for load level i; and A_j denotes the lateral area of pile section j, with the lateral area of a pile section with a root taken to be the lateral area of the corresponding equal-diameter pile in the same location.

The lateral friction resistance diagrams of root piles at different root buried depths are shown in Fig. 2D–F. The lateral friction resistance of

the upper part of the pile body without root increases gradually with the increase of depth in each group of test piles, and all of them produce the relative maximum value of lateral friction resistance at the root. The difference is that when the root is buried at a depth of 260 mm, the maximum value of lateral friction resistance is generated at the root at a depth of 430 mm, which is smaller than that at the root, and the lateral friction resistance at the lower part of the pile body decreases sharply. When the buried depth of the root is 340 mm, the lateral friction resistance of the pile body below the root decreases sharply. The maximum value of the lateral friction resistance of the pile section without the root occurs at a depth of 190 mm on the pile body. This value is smaller than the maximum value of the side friction resistance at the root. When the buried depth of the root is 420 mm, the lateral friction resistance of the pile body under the root decreases sharply, and the maximum value of the lateral friction resistance of the pile section without root appears at the depth of 260 mm on the pile body, which is deeper than the condition of the buried depth of the root is 340 mm. The reason for the above phenomenon may be that the side friction exerted downward from the top, and the deeper the depth, the greater the soil pressure. Therefore, the side friction of the section without root on the pile body gradually increases with the increase of depth. The end resistance provided by the surface of the root and the side friction provided by the section with equal diameter are greater than the side resistance provided by the section with equal diameter, so the extreme value of side friction resistance appears at the root. The squeezing effect of the root on the soil above will change the compaction of the soil around the pile. When the buried depth is deeper, the squeezing effect of the root increases. This, along with the soil pressure, causes the characteristics of the soil above to form a dense region. In this region, there will be a relative maximum value of the soil pressure. This part of the analysis will be explained later in the soil pressure analysis. Therefore, when the root buried depth is 340 mm and 420 mm, the rootless pile section shows a relative maximum value of lateral resistance. when the root buried depth is 340 mm and 420 mm, the lateral friction of the pile section without root appears to have a relative maximum value of resistance. When the root buried depth is 260 mm, due to the small buried depth, the rootless pile section does not produce the relative maximum value of lateral friction resistance, however, due to the pile body of the rootless area below the pile to the surrounding soil body of the extrusion effect makes the bottom of the pile body also produces the relative maximum value of lateral friction resistance. The loosening of the soil in the lower part of the root and the very bottom of the pile resulted in a sharp decrease in the lateral friction resistance of the pile in those areas.

3.4. Proportion of load carried by the root segment

Root bearing percentage is the proportion of the load borne by the root pile section to the total load, calculated as shown in formulas (3) and (4).

$$\eta_{i-total} = \sum_{j=1}^{x} \eta_{ij} \tag{3}$$

$$\eta_{ij} = \frac{F_{ij}}{Q_i} \tag{4}$$

In the formula, η_{ij} is the percentage of the total load carried by the j root segment under the i load level; F_{ij} is the amount of attenuation of the axial force in the j root segment under the i load level; Q_i refers to the value of the total load in the i level; $\eta_{i-total}$ is the total percentage of the load carried by all the root segments under the i load level; x denotes that there is a total of the x levels of loading.

Root pile section bearing ratio is the ratio of the attenuation value of the axial force in the root pile section to the total load, which can reflect the effect of the root to enhance the uplift bearing capacity of the pile and the process of the bearing capacity of the root section, so as to reveal the bearing mechanism of the root pile. Fig. 3A shows the bearing ratio of the root pile section under different root buried depths. It can be seen that the bearing ratio of the root segment of the root pile with root buried depths of 260 mm, 340 mm and 420 mm ranges from 12.33% to 15.68%, 9.98%–17.82 % and 6.98%–21.65%, respectively. The smaller the root buried depth is, the higher is the bearing ratio of the root segment at the beginning of the loading process, and the bigger the root buried depth is, the bigger is the final bearing ratio of the root. In the middle of loading, the load carrying ratio of the root section with large root buried depth gradually exceeds the load carrying ratio of the root section with small root buried depth. The reason for the above phenomenon may be that the lateral friction resistance is exerted from top to bottom, and the smaller the root buried depth is, the more it acts first, so the smaller the root buried depth is, the higher the ratio of the root section at the beginning of loading is. The greater the root buried depth, the more obvious the enhancement of the ultimate bearing capacity of the root pile, so the greater the final bearing ratio of the root. In the middle of loading, the soil body near the upper part of the pile without root pile section gradually undergoes shear damage, and the root pile section gradually plays a role, and the greater the root buried depth is, the more load it can bear, so the load carrying ratio of the root pile section with a large root buried depth gradually exceeds the load carrying ratio of the root pile section with a small root buried depth.

3.5. Earth pressure around the pile

The soil pressure around the pile with different root buried depths (the test measured the change of soil pressure during loading) is shown in Fig. 2G–I. The trend of soil pressure around the pile with different root buried depths is more or less the same, which is first increasing and then decreasing to a negative value, the reason may be that the pile body has a compacting effect on the upper soil, and the soil at the bottom of the pile body is loosened due to the uplift displacement of the pile body.

The difference is that, in terms of the location of the maximum earth pressure, the maximum earth pressure around the root pile with a root buried depth of 260 mm is located at a depth of 180 mm, and the maximum earth pressure around the root pile with root buried depths of 340 mm and 420 mm is located at a depth of 260 mm. The reason for this may be that the squeezing effect of the root on the soil above it changes the compaction of the soil above it, and the greater the buried depth of the root is, the densest point of the squeezing will be shifted upward.

In terms of the scope of the squeeze zone, in the late loading stage of the root pile with a root buried depth of 260 mm, the soil around the pile above the depth of 340 mm is in a squeeze state (soil pressure is positive); for the root pile with a root buried depth of 340 mm, the soil around the pile above the depth of 260 mm is in a squeeze state (soil pressure is positive); for the root pile with a root buried depth of 420 mm, the soil around the pile above the depth of 340 mm is in a squeeze state (soil pressure is positive) in the late loading stage. It can be seen that the soil surrounding the pile with a root buried depth of 420 mm has the largest compacted zone, followed by the pile with a root buried depth of 260 mm, and the soil surrounding the pile with a root buried depth of 340 mm has the smallest compacted zone. The reason may be that, when the root buried depth is larger, the range of soil above the root squeezing is naturally larger, when the root buried depth is smaller, in addition to the root squeezing the soil above the root, the pile section without root in the lower part of the pile body will also drive the soil around the pile and thus squeezing the soil around the pile, so the soil around the pile of the root with the root buried depth of 340 mm has the smallest squeezing area.

In terms of soil compaction degree around the pile, under the last stage of load, the earth pressure in the compaction area around the pile with the root buried depth of 260 mm is the smallest, which is 2.16 kPa; the earth pressure in the compaction area around the root pile with the

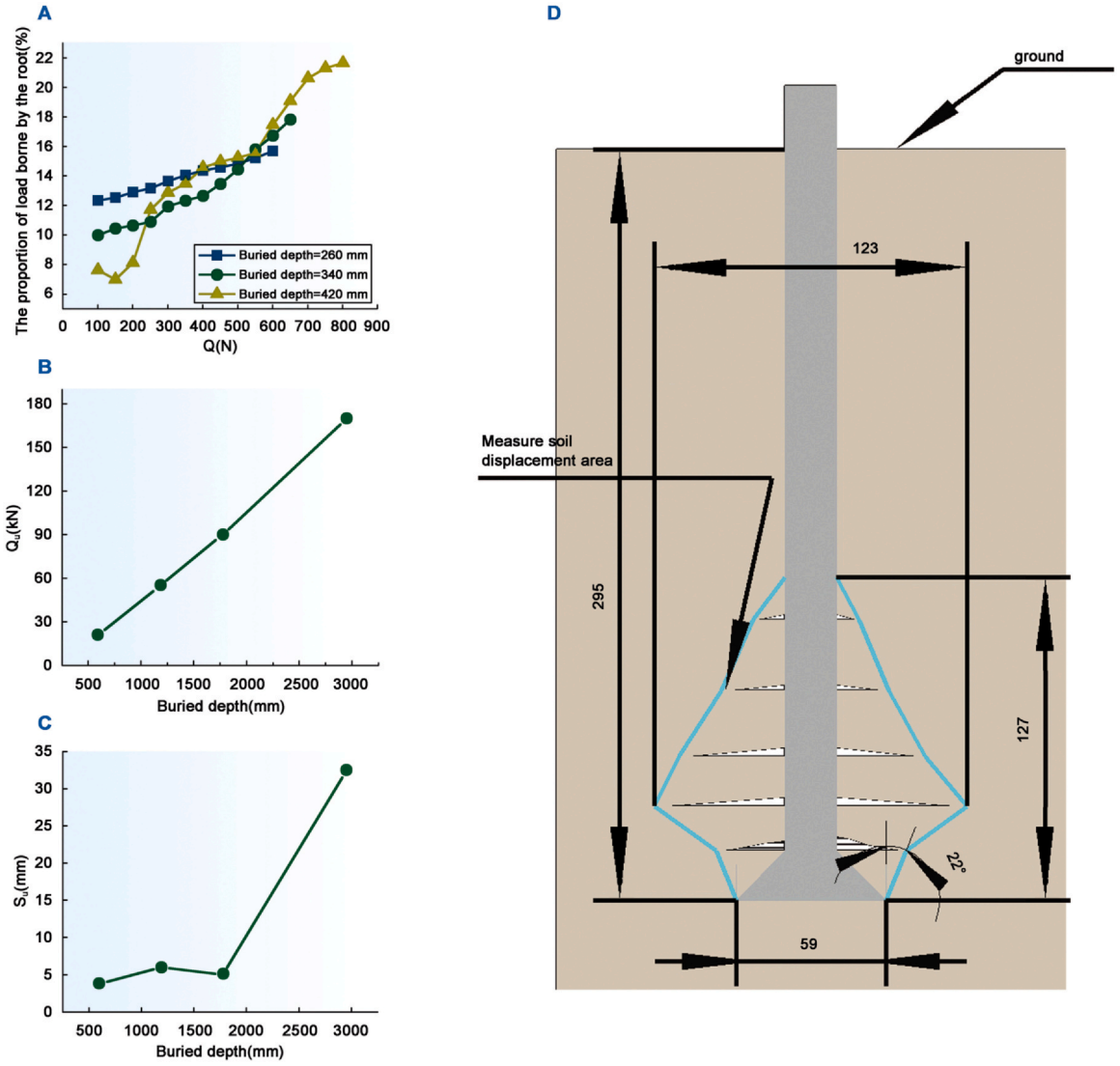

Fig. 3. (**A**) Bearing ratios of root at root pile segments for different root buried depths; (**B**) Plot of ultimate bearing capacity of spread footing pile against depth of spread footing portion in previous study (Chen et al., 2010); (**C**) Plot of ultimate displacement of spread footing pile against depth of spread footing portion in previous study (Chen et al., 2010); (**D**) Map of the area where the soil displacement occurred on the measured soil of the spread footing piles in the previous study (Chen et al., 2010).

root buried depth of 420 mm is the largest, which is 5.43 kPa; and the earth pressure in the compaction area around the root pile with the root buried depth of 340 mm is 4.72 kPa. The reason may be that the greater the buried depth of the root, the greater the ultimate uplift bearing capacity, the more the load borne by the root pile section, the greater the extrusion pressure on the soil.

4. Discussion

In summary, increasing the buried depth of the root significantly enhances the pullout bearing capacity of root piles and improves their ability to control uplift displacement. However, once the buried depth reaches a certain point, the increase in displacement control capability becomes minimal. The ultimate uplift displacement S_u initially increases and then decreases with greater buried depth. There exists an optimal buried depth, or a range of depths, that can substantially enhance the pullout bearing capacity of the pile foundation while maintaining relatively small ultimate displacement. Additionally, the attenuation of axial force at the root exhibits a step-like pattern. As the buried depth of the root increases, the area of compacted soil expands, and the maximum soil pressure value shifts upward.

In the study of root piles resisting uplift displacement pattern, previous study (Ge et al., 2019) carried out the bearing capacity and displacement analysis of root piles with different root buried depths in silica sand foundation. In the study of uplift displacement field of pile foundation, previous study (Chen et al., 2010) gives the uplift displacement region of expanded bottom pile and reveals the uplift damage mode of expanded bottom pile. This paper is compared with the above studies as follows:

(1) In terms of vertical bearing capacity of piles. Previous study (Ge et al., 2019) gives the Q-S curves of uplift of root piles with the upper layer of root piles 230 mm, 310 mm and 390 mm from the surface of sandy soil, and it is found that the greater the depth of buried, the greater the ultimate load bearing capacity of resistance to uplift, and the greater the total uplift displacement of the pile body. Previous study (Ge et al., 2019) only compared the total uplift displacement of the pile body, but did not compare the ultimate uplift displacement corresponding to the ultimate load bearing capacity. In this paper, the pattern of the ultimate bearing capacity against uplift and the total uplift displacement of the pile is the same as that in the previous study (Ge et al., 2019). In addition, this paper points out that after the root buried depth is increased to a certain degree, the enhancement of displacement control ability is

Table 3
Comparison of theoretical calculation and test results of ultimate bearing capacity for pullout resistance.

Buried depth (mm)	Test results $Q_u(N)$	$Q_u(N)$	Error
260	450	527.70	17.27%
340	500	584.34	16.87%
420	550	640.98	16.54%

not large, and the ultimate uplift displacement S_u increases and then decreases with the depth of buried, and there exists the optimal buried depth or the range of buried depth that can greatly enhance the pile foundation's resistance to uplift load bearing capacity, and at the same time the ultimate displacement is relatively small, which can be a useful guide to the design of root piles in practical engineering. There exists an optimum buried depth or range of buried depth that can greatly improve the pile foundation's pullout capacity while the ultimate displacement is relatively small, which is of great significance in guiding the design of root piles in actual projects. However, this paper does not give a quantitative judgment method for the optimum buried depth and the range of buried depth, which needs to be further studied.

(2) Previous study (Wang et al., 2024) proposed a formula for calculating the ultimate bearing capacity of root piles resisting pullout in sandy soils, as shown in Eq. (5). The ultimate bearing capacity resisting pullout in Eq. (5) Q_u consists of the lateral friction force of the pile body Q_{sp}, the lateral friction force of the root Q_{sr}, the end resistance force of the root on the upper surface of the root Q_{er}, and the gravity force of the pile body W_p, and the explanations of each variable are described in detail in previous study (Wang et al., 2024), which will not be repeated here. The results of the tests in this paper are compared with those calculated using the formulae in the previous study (Wang et al., 2024), and the results are shown in in Table 3. From in Table 3, it can be seen that the theoretical calculation results are overall large, with an error of about 16%. This may be due to the special engineering properties of coral sand, and this aspect needs to be further studied.

$$Q_u = Q_{sp} + Q_{sr} + Q_{er} + W_p \tag{5}$$

$$Q_{sp} = \pi d \sum_{g=1}^{f} \int_{L_{g1}}^{L_{g2}} (K_{ug}\gamma_g \tan\varphi_g) z dz = \pi d \sum_{g=1}^{f} \left[\left(\frac{L_{g1} + L_{g2}}{2} \right) K_{ug}\gamma_g \tan\varphi_g \right] \cdot H_g \tag{6}$$

$$Q_{sr} = \eta_r \sum_{j=1}^{n} \int_{L_{j1}}^{L_{j2}} 2ml(K_{uj}\gamma_j \tan\varphi_j) z dz = 2\eta_r mhl \sum_{j=1}^{n} \left(\frac{L_{j1} + L_{j2}}{2} \right) K_{uj}\gamma_j \tan\varphi_j \tag{7}$$

$$Q_{er} = \eta_r mbl \sum_{j=1}^{n} \bar{\sigma}_{vj}(S_{qj}N_{qj}) \tag{8}$$

$$N_{qj} = e^{\pi \tan\varphi_j} \tan^2\left(45^\circ + \frac{\varphi_j}{2}\right) \tag{9}$$

$$S_{qj} = 1 + \frac{b}{l}\tan\varphi_j \tag{10}$$

$$\eta_r = \begin{cases} \dfrac{\left(\frac{s}{l}\right)^{0.015m+0.45}}{0.15n + 0.1m + 1.9}, & 4 < \frac{s}{l} < 8 \\ 1, & \frac{s}{l} \geq 8 \end{cases} \tag{11}$$

(3) In the study of pile bearing capacity and displacement patterns. Previous study (Chen et al., 2010) carried out a large-size modeling test study on the uplift bearing capacity of expanded bottom piles in unsaturated floury soil with different buried depths. The tables of the uplift ultimate bearing capacity and uplift ultimate displacement of the expanded bottom pile in relation to the buried depth of the expanded bottom portion were plotted as shown in Fig. 3B and C, respectively. From Fig. 3B, it can be seen that the pile foundation pullout capacity increases with the increase of the depth of the expanded head, which is similar to the test results in this paper, and the pile foundation pullout capacity can be improved by increasing the depth of the expanded head or the root. It can be seen from Fig. 3C, the ultimate displacement of the expanded pile with the expansion of the head buried depth increases first basic unchanged after a sharp increase, it can be presumed that the expanded pile also exists in the higher bearing capacity, while the ultimate displacement of the smaller buried depth range, this law and the laws derived from this paper are generally consistent with the law. It can be seen that for the root piles and spread footing piles, which are designed to improve the pullout capacity by means of pile body members, the optimum buried depth range exists in which the pile body members have a high pullout capacity and a small pullout ultimate displacement at the same time.

(4) In the study of uplift displacement field of pile foundation. Previous study (Chen et al., 2010) gives the uplift displacement region of expanded bottom pile and reveals the uplift damage mode of expanded bottom pile. In previous study (Chen et al., 2010), the measured displacement region of soil body of expanded pile is shown in Fig. 3D, from which it can be seen that the displacement region above the expanded head of expanded pile shows the law of increasing first and then decreasing along the depth direction, which also reflects that the displacement of soil body increases first and then decreases along the depth, and then it can be presumed that the change of soil pressure around the pile also increases first and then decreases along the depth. This law is consistent with the law in this paper, which indicates that the root and the enlarged head play the same role of driving the surrounding soil body to carry the load together.

5. Conclusions

In this paper, the pullout bearing characteristics of root piles in coral sand foundations with different root buried depths are comparatively analyzed through model tests. The main conclusions are as follows.

(1) Increasing the root buried depth can improve the root pile's ability to resist elevation bearing capacity and control upward elevation displacement, and there exists an optimal buried depth or range of embedment depths that can effectively improve the pile foundation's ability to resist elevation bearing capacity and control the ultimate displacement.

(2) The root carries most of the load. When the root is buried at a large depth, the maximum value of lateral friction resistance occurs at the upper part of the pile body without root, and when the root is buried at a small depth, the maximum value of lateral friction resistance occurs at the lower part of the pile body without root.

(3) The range of bearing ratio of root section of root piles with root buried depths of 260 mm, 340 mm and 420 mm are 12.33%–15.68%, 9.98%–17.82% and 6.98%–21.65%, respectively; the smaller the root buried depth is, the higher is the ratio of bearing ratio of the root section at the beginning of loading, and the bigger the root buried depth is, the bigger is the ratio of final bearing ratio of the root.

(4) The amount of change of soil pressure around the pile first increases and then decreases. The soil around the upper part of the pile body is crowded, the soil around the lower part of the pile body will be loosened; the root buried depth increases, the densest point of the crowded (the maximum value of the soil pressure) will move upward, and the crowded area of the soil will first decrease and then increase.

CRediT authorship contribution statement

Xiangwei Fang: Writing – review & editing, Supervision, Project administration, Methodology, Funding acquisition, Formal analysis, Data curation. **Yaoyi Zhang:** Writing – review & editing, Writing – original draft, Methodology, Investigation, Formal analysis, Data curation. **Zhiqiang Wang:** Writing – review & editing, Writing – original draft, Methodology, Investigation, Formal analysis, Data curation. **Peixi Xiong:** Formal analysis, Data curation. **Fenghui Hu:** Investigation, Data curation. **Ganggang Zhou:** Investigation. **Chunyan Wang:** Investigation.

Data availability

Data will be made available on request.

Appendices

Equation

$$F_{\mathrm{N}} = EA\varepsilon \tag{1}$$

$$q_{sij} = \frac{F_{ij}}{A_j} \tag{2}$$

$$\eta_{i-total} = \sum_{j=1}^{x} \eta_{ij} \tag{3}$$

$$\eta_{ij} = \frac{F_{ij}}{Q_i} \tag{4}$$

$$Q_{\mathrm{u}} = Q_{\mathrm{sp}} + Q_{\mathrm{sr}} + Q_{\mathrm{er}} + W_{\mathrm{p}} \tag{5}$$

$$Q_{\mathrm{sp}} = \pi \mathrm{d} \sum_{g=1}^{f} \int_{L_{g1}}^{L_{g2}} (K_{ug}\gamma_g \tan\varphi_g) z \mathrm{d}z = \pi \mathrm{d} \sum_{g=1}^{f} \left[\left(\frac{L_{g1} + L_{g2}}{2} \right) K_{ug}\gamma_g \tan\varphi_g \right] \cdot H_g \tag{6}$$

$$Q_{\mathrm{sr}} = \eta_{\mathrm{r}} \sum_{j=1}^{n} \int_{L_{j1}}^{L_{j2}} 2ml(K_{uj}\gamma_j \tan\varphi_j) z \mathrm{d}z = 2\eta_{\mathrm{r}} mhl \sum_{j=1}^{n} \left(\frac{L_{j1} + L_{j2}}{2} \right) K_{uj}\gamma_j \tan\varphi_j \tag{7}$$

$$Q_{\mathrm{er}} = \eta_{\mathrm{r}} mbl \sum_{j=1}^{n} \bar{\sigma}_{vj} (S_{qj} N_{qj}) \tag{8}$$

$$N_{qj} = \mathrm{e}^{\pi \tan\varphi_j} \tan^2 \left(45^\circ + \frac{\varphi_j}{2} \right) \tag{9}$$

$$S_{qj} = 1 + \frac{b}{l} \tan\varphi_j \tag{10}$$

$$\eta_{\mathrm{r}} = \begin{cases} \dfrac{\left(\frac{s}{l}\right)^{0.015m+0.45}}{0.15n + 0.1m + 1.9}, & 4 < \frac{s}{l} < 8 \\ 1, & \frac{s}{l} \geq 8 \end{cases} \tag{11}$$

Declaration of Competing Interest

Yaoyi Zhang is employed by CCCC Yangtze River Construction Development Group Co., Ltd., and the other authors declare that they have no known competing financial interests or personal relationships that could have appeared to influence the work reported in this paper.

Acknowledgements

The research was financially supported by National Natural Science Foundation of China (No. 51978103, No. 52408355), the Postdoctoral Fellowship Program of CPSF (No. BX20240450), and Chongqing Talent Innovation and Entrepreneurship Demonstration Team (No. cstc2024ycjh-bgzxm0012), the authors gratefully acknowledge this financial support.

References

Aamer, F., Azzam, W., Farouk, A., Nasr, A., & Nazir, A. (2023). Utilization of blade anchor for improving the uplift capacity of pile in sand: model study. *Ocean Engineering, 278*. https://doi.org/10.1016/j.oceaneng.2023.114435

Chen, R. P., Zhang, G. Q., Kong, L. G., Chen, Y. M., Xing, Y. L., & Ying, J. G. (2010). Large-scale tests on uplift ultimate bearing capacities of enlarged base piles in saturated and unsaturated silty soils. *Chinese Journal of Rock Mechanics and Engineering, 2905*, 1068–1074 (in Chinese).

Fang, X. W., Hu, F. H., Yao, Z. H., Chen, Z. H., & Shen, C. N. (2023). Development and application of triaxial apparatus for soil with high bearing pressure by computed tomography. *Journal of Testing and Evaluation, 22*. https://doi.org/10.1520/jte20220584

Fang, X. W., Shen, C. N., Chu, J., Wu, S. F., & Li, Y. S. (2015). An experimental study of coral sand enhanced through microbially-induced precipitation of calcium carbonate. *Rock and Soil Mechanics, 3610*, 2773–2779. https://doi.org/10.16285/j.rsm.2015.10.005

Fang, X. W., Wang, Z. Q., Shen, C. N., Chen, C., & Yao, Z. H. (2024). Study on the pullout bearing characteristics of root piles in coral sand foundations under different water content states. *Applied Ocean Research, 146*, Article 103962. https://doi.org/10.1016/j.apor.2024.103962

Ge, N., Sun, Y., Hou, C., Zhu, D., & Yin, Y. (2019). Model test on rooted uplift pile in sand (in Chinese) *Journal of Yangtze River Scientific Researeh Institute, 3608*, 146–152. https://doi.org/10.11988/ckyyb.20180059

Gong, X. N. (2015). *Pile foundation engineering manual*. Beijing: China Architecture & Building Press (in Chinese).

Gong, W., Wang, L., & Yin, Y. (2015). Applied and experimental study on the root foundation in the thick covering stratum region. *China Civil Engineering Journal, 48*, 69–75 (in Chinese).

Gui, F. K., Kong, J. Q., Feng, D. J., Qu, X. Y., Zhu, F., & You, Y. (2021). Uplift resistance capacity of anchor piles used in marine aquaculture. *Scientific Reports, 11*, 111. https://doi.org/10.1038/s41598-021-99817-5

Hu, F. H., Fang, X. W., Shen, C. N., Yao, Z. H., Zhou, G. G., & Wang, Z. Q. (2023a). Discrete element numerical analysis for bearing characteristics of coral sand

foundation considering particle breakage. *Marine Georesources Geotechnology*. https://doi.org/10.1080/1064119X.2023.2233505

Hu, F., Gong, W., Tong, X., Yin, Y., & Shan, J. (2010). Analysis of bearing capacity of root-caisson with flexual roots. *Chinese Journal of Computational Mechanics, 2703*, 505–510 (in Chinese).

Hu, F. H., Fang, X. W., Yao, Z. H., Wu, H. R., Shen, C. N., & Zhang, Y. T. (2023b). Experiment and discrete element modeling of particle breakage in coral sand under triaxial compression conditions. *Marine Georesources Geotechnology, 412*, 142–151. https://doi.org/10.1080/1064119x.2021.2019356

Lei, J. T., Zhou, Z. J., Han, D. D., Zhu, S. S., Feng, H. M., Wang, K. C., & Tian, Y. Q. (2022). Centrifuge model tests and settlement calculation of belled and multi-belled piles in loess area. *Soil Dynamics and Earthquake Engineering, 161*, 17. https://doi.org/10.1016/j.soildyn.2022.107425

Li, Z., Hu, P., Ma, J., Gao, M., Huang, H., Liu, X., ... Sun, Z. (2022). Analysis and prospect of offshore Wind power development in China. *China Offshore Oil and Gas, 345*, 229–236 (in Chinese).

Liu, C., Ji, F., Song, Y., Wang, H. T., Li, J. H., Xuan, Z. T., Zhao, M. Z., & Greco, A. (2023). Upper bound analysis of ultimate pullout capacity for a single pile using hoek-brown failure criterion. *Buildings, 1312*(16), https://doi.org/10.3390/buildings13122904

Liu, W., Xu, H. Y., & Chen, L. Z. (2011). Analytic calculation of load-displacement for uplift piles using hyperbolic transfer function. *Materials Research Innovations, 15*, S569–S572. https://doi.org/10.1179/143307511x12858957676795

Luo, X. G., Ren, W. X., Yin, Y. G., & Yu, Y. C. (2022). A modified hyperbolicity-based load transfer model for nonlinear settlement analysis of root piles in multi-layered soils. *Acta Geotechnica, 171*, 303–317. https://doi.org/10.1007/s11440-021-01215-8

Luo, X. G., Ren, W. X., Yin, Y. G., & Yu, Y. C. (2022). An extended BNWF model for root piles incorporating soil-root interactions under lateral loading. *Computers and Geotechnics, 152*, 13. https://doi.org/10.1016/j.compgeo.2022.105039

Ma, J., Wang, R., Hu, Z., Mu, T., Liu, A., & Olusegun, V. T. (2023). Calculation method of bearing capacity of screw pile under compression load based on limit equilibrium theory. *Proceedings of the Institution of Civil Engineers-Geotechnical Engineering*. https://doi.org/10.1680/jgeen.22.00122

Ma, H. W., Wu, Y. Y., Tong, Y., & Jiang, X. Q. (2020). Research on bearing theory of squeezed branch pile. *Advances in Civil Engineering, 2020*, 12. https://doi.org/10.1155/2020/6637261

Malik, A. A., Kuwano, J., Tachibana, S., & Maejima, T. (2019). Effect of helix bending deflection on load settlement behaviour of screw pile. *Acta Geotechnica, 145*, 1527–1543. https://doi.org/10.1007/s11440-019-00778-x

Ministry of Housing and Urban-Rural Development of the People's Republic of China. (2014). *Technical specification for testing building foundation piles*. Beijing: China Architecture & Building Press.

Moayedi, H., & Mosallanezhad, M. (2017). Uplift resistance of belled and multi-belled piles in loose sand. *Measurement, 109*, 346–353. https://doi.org/10.1016/j.measurement.2017.06.001

Moayedi, H., & Rezaei, A. (2019). An artificial neural network approach for under-reamed piles subjected to uplift forces in dry sand. *Neural Computing Applications, 312*, 327–336. https://doi.org/10.1007/s00521-017-2990-z

Mu, L., Huang, M., Gong, W., & Yin, Y. (2010). Response analysis of anchorage foundation under lateral loading (in Chinese) *Rock Soil Mech, 311*, 287–292. https://doi.org/10.16285/j.rsm.2010.01.050

Peng, Y., Liu, H. L., Li, C., Ding, X. M., Deng, X., & Wang, C. Y. (2021). The detailed particle breakage around the pile in coral sand. *Acta Geotechnica, 166*, 1971–1981. https://doi.org/10.1007/s11440-020-01089-2

Polishchuk, A. I., & Maksimov, F. A. (2018). Engineering method of calculating the settlement of two-bladed screw pile in clayey soil. *Soil Mechanics and Foundation Engineering, 546*, 377–383. https://doi.org/10.1007/s11204-018-9484-6

Qi, C. G., Liu, G. B., Wang, Y., & Deng, Y. B. (2015). Theoretical study on setup of expanded-base pile considering cavity contraction. *Journal of Central South University, 2211*, 4355–4365. https://doi.org/10.1007/s11771-015-2984-x

Vignesh, V., & Muthukumar, M. (2023). Experimental and numerical study of group effect on the behavior of helical piles in soft clays under uplift and lateral loading. *Ocean Engineering, 268*, 18. https://doi.org/10.1016/j.oceaneng.2022.113500

Wang, Z. Q., Fang, X. W., Li, Y. H., Shen, C. N., Hu, F. H., & Zhou, G. G. (2023). Investigation into pullout characteristics of root piles within coral sand foundations at varied relative compaction. *Marine Georesources Geotechnology,* 1–16. https://doi.org/10.1080/1064119X.2023.2287694

Wang, Z. Q., Fang, X. W., Yao, Z. H., Zhou, G. G., Lin, X. L., & Shen, C. N. (2024). Investigating the influence of root layer quantity on the pullout bearing characteristics of root piles in coral sand foundations. *Ocean Engineering, 293*, Article 116616. https://doi.org/10.1016/j.oceaneng.2023.116616

Wang, R., Song, C., & Zhao, H. (1997). *Coral reef engineering geology of Nansha Islands.* Beijing: Science Press (in Chinese).

Yancheng, Y., Weixin, R., Yonggao, Y., & Xiaoguang, L. (2023). Vertical load transfer mechanism and ultimate bearing capacity calculation of root pile foundation. *Journal of Building Structures, 447*, 1–13 (in Chinese).

Yao, W. J., & Chen, S. P. (2014). Elastic-plastic analytical solutions of deformation of uplift belled pile. *Tehnicki Vjesnik-Technical Gazette, 216*, 1201–1211.

Yao, W. J., & Xiao, L. (2019). Analytical solutions of deformation of uplift belled group piles considering reinforcement effect. *Ksce Journal of Civil Engineering, 233*, 1007–1016. https://doi.org/10.1007/s12205-019-1635-4

Yin, Y. (2007). Scheme conception of root foundation and anchor block. *Highway, 512*, 46–49 (in Chinese).

Yin, Y. (2015). *Root foundation.* Beijing: China Communication Press (in Chinese).

Yu, Y., Ren, W., Yin, Y., & Luo, X. (2023). Vertical load transfer mechanism and ultimate bearing capacity calculation of root pile foundation. *Journal of Building Structures, 447*, 1–13 (in Chinese).

Zhang, J., Huang, X., Wei, L., Zhou, J., Yuan, J., & Wang, X. (2020). Research on visual model test of displacement distribute characteristics and load transfer model of root pile during uplifting (in Chinese) *Journal of China Coal Society*. https://doi.org/10.13225/j.cnki.jccs.2019.0962

Zhang, M. X., Xu, P., Cui, W. J., & Gao, Y. B. (2018). Bearing behavior and failure mechanism of squeezed branch piles. *Journal of Rock Mechanics and Geotechnical Engineering, 105*, 935–946. https://doi.org/10.1016/j.jrmge.2017.12.010

Zhou, J., Huang, X., Zhang, J., Wei, L., & Yuan, J. (2021). Experimental investigation of the uplift and lateral bearing capacity of root piles. *Soil Mechanics and Foundation Engineering, 576*, 473–479. https://doi.org/10.1007/s11204-021-09695-2